Abiotic reduction of antimony(V) by green rust

$(Fe_4(II)Fe_2(III)(OH)_{12}SO_4 \cdot 3H_2O)$

Satoshi Mitsunobu
(Ph D student 3rd)

Department of Earth and Planetary Systems Science, Graduate School of Science, Hiroshima University, Higashi-Hiroshima, Hiroshima 739-8526, Japan

Proposal No.: 2006B1704
Proposal title: A study on the kinetics of redox reactions of As and Sb at the solid-water interface using quick XAFS technique
Beam-line: BL01B1

1. Introduction

Antimony (Sb) is a toxic element widely distributed in the lithosphere and mainly associated with arsenic (As) as sulfide or oxide. Antimony compounds are considered to be pollutants of high interest by the United States Environmental Protection Agency (1979) and the European Union (1976). However, the geochemical behavior of Sb in soil and sediment is still largely unknown. Antimony belongs to group 15 of the periodic table below As and can exist in four oxidation states (−III, 0, III, and V), though Sb(III) and Sb(V) are the most frequently encountered species in the environment. To a great extent, the behavior of Sb in the environment depends on its oxidation state. Moreover, the toxicity of inorganic Sb is assumed to be similar to that of As and also depends on the oxidation state; Sb(III) is more toxic than Sb(V) (Picard and Bosco, 2003). Although very few sorption studies of Sb on natural sorbents have been reported to date, the major host phase of Sb in natural soil and sediment is Fe hydroxide (Chen et al., 2003; Scheinost et al., 2006; Mitsunobu et al., 2006). Mitsunobu et al. (2006) reported that Sb can exist as the oxidized form, Sb(V), over a wide redox range in soil, suggesting that Sb(V) is a stable form in the environment, while the oxidation state of As changes readily depending on the redox condition.

Green rusts are layered Fe^{II}-Fe^{III} hydroxides that have a pyroaurite-type structure consisting of alternating positively charged hydroxide layers and hydrated anion layers. Isomorphic substitution of Fe^{3+} for Fe^{2+} in the trioctahedral sheets of $Fe(OH)_2$ confers a positive charge to the hydroxide layer that is balanced by hydrated anions in the interlayer (typically Cl^-, SO_4^{2-}, or CO_3^{2-}). Green rusts are formed by a number of abiotic and biotic processes under circumneutral to alkaline conditions in suboxic environments. They have been initially identified as products of both abiotic and microbially induced corrosion of iron and steel (Bigham and Tuovinen, 1985; Génin et al., 1998; Kumar et al., 1999; Refait et al., 1998).

Green rusts may be important for trace metal mobility in the environment because of their high reactive surface areas and their potential to reduce metal species such as Se(VI), Cr(VI), and U(VI) (Myneni et al., 1997; Loyaux-Lawniczak et al., 2000; O'Loughlin et al., 2003). Hansen et al. (1996) have also shown that sulphate green rust is capable of reducing nitrate to ammonium. On the other hand, it is also reported that sulphate green rust cannot reduce As(V) to As(III) (Randall et al., 2001) and that As(III) is partially oxidized to As(V) by carbonate green rust (Su and Puls, 2004). Thus, the reducing potential of green rust greatly depends on its reactant. The reduction of Sb(V) to Sb(III) is important for the toxicology and environmental chemistry of Sb, since Sb(III) is more toxic than Sb(V) and Sb mobility depends on its oxidation state. However, the interactions between Sb(V) and any green rusts have not been studied previously.

The objective of this work is to thus understand the interactions (sorption and reduction)

between Sb(V) and green rust phases, as well as to examine whether green rust can reduce the stable Sb(V). Subsequently, we investigate the influence of green rust upon Sb behavior in the environment. Accordingly, we employed X-ray absorption fine structure (XAFS) analysis to determine directly the oxidation state of Sb sorbed on green rust, while we also determined the Sb(III)/Sb(V) ratio in water phase by high performance liquid chromatography connected to ICP-MS (HPLC-ICP-MS).

2. Materials and methods

2. 1. Reaction of Sb(V) with green rust

The methods of Schwertmann and Fechter (1994) and Heasman et al. (2003) were followed to prepare sulphate green rust with the expected approximate bulk formula $Fe^{II}_2Fe^{III}(OH)_5(SO_4)$. The green rust samples were not exposed to light during preparation and analysis to prevent unwanted photoredox reactions. The sample was prepared in a 500 mL glass vessel in a water bath maintained at 25±0.1°C. The vessel containing a magnetic stirrer was capped by an airtight PVC lid with holes for pH electrode, a gas inlet/outlet port, and a sample port.

Initially, 370 mL of Milli-Q water was added to the vessel and purged with N_2(g) for 48 h to remove dissolved oxygen before the addition of 20.57 g of $FeSO_4 \cdot 7H_2O$. Once pH in the solution reached pH 7.0 by the addition of a CO_2-free 1.0 M NaOH solution, the N_2(g) flow was replaced with laboratory air supplied by a small pump via an open-ended glass tube. Since the oxidation/hydrolysis reaction liberates protons, a titrator (Metrohm 665 Dosimat) was used to constantly add a 1.0 M NaOH solution throughout the reaction and maintain pH at 7.0 ± 0.1.

Sampling was achieved with a 10 ml plastic pipette, and the suspension collected was transferred immediately to a 50 mL screw-top polypropylene centrifuge tube that was filled to the brim without any air trapped inside. Here, we define the reaction time of Fe(II) oxidation as T_R. The dark green suspension was first sampled after 30 min (T_R = 0.5 h). At T_R = 0.83 h (50 min), 10 mL of a 1500 mg/L Sb(V) stock solution prepared from $K[Sb(OH)_6]$ (Wako, Japan) was added. Subsequently, the suspension samples were taken at T_R = 1.0, 1.5, 2.0, and 2.5 h. After the final sampling at T_R = 2.5 h, all the samples were centrifuged and filtered through 0.22 μm membrane filters in a N_2 purged glove box. The filtrates were then stored in the dark at 4°C until analysis. The Sb(III)/Sb(V) ratio in the filtrate were then measured by HPLC-ICP-MS on the sampling day. All of the collected green rust samples were packed into polyethylene bags for XAFS analysis under N_2 and frozen immediately in liquid N_2 to prevent oxidation during storage.

2. 2. X-ray diffraction analysis

The mineralogy of collected samples was determined by X-ray diffractometer (XRD; MAC Sci., M18XHF) using Cu K_α radiation with monochromator before the detector. The XRD slides were prepared by drying a glycerol-based suspension of each sample onto small glass discs in the N_2 purged glovebox. The obtained viscous paste could protect the air-sensitive samples against oxidation during XRD analysis (Hansen et al., 1999). A comparison of the relative intensity of observed green rust and lepidocrocite diffraction peaks allowed a qualitative assessment of the rate of green rust oxidation.

2. 3. Water analysis

Total Fe and Sb abundances in the filtrates were measured by graphite-furnace atomic absorption spectroscopy (Shimadzu AA6650) and ICP-MS (Thermoelectron, PQ-3), respectively. The precision of the measurement was better than 5% for both Fe and Sb. The Sb(III)/Sb(V) ratio in the solution was determined by HPLC-ICP-MS. The pump and oven used were a Pu-2089 Plus (JASCO) and a Co-2065 Plus (JASCO), respectively. The experimental conditions were the same as those described by Krachler and Emons (2001), and an anion exchange column (PRP-X100, Hamilton; 250 mm × 4.1 mm) was used at 40°C. The mobile phase was a 20 mM EDTA (Wako, Japan) solution at pH 4.7. The flow rate was 0.25 mL/min. Two standard solutions of Sb(III) and Sb(V) were prepared by dissolving appropriate amounts of potassium antimony tartrate (Wako, Japan) and $K[Sb(OH)_6]$ in Milli-Q water, respectively.

2. 4. XANES measurement

Antimony L_I-edge X-ray absorption near-edge structure (XANES) was measured at beamline BL-9A at Photon Factory, Tsukuba, Japan (Nomura and Koyama, 2001). A Si(111) double-crystal monochromator was used, and the beam was focused using a pair of bent conical mirrors coated with Rh, where the contribution of higher harmonic components was negligible. The fluorescence X-ray was measured using a 19-element Ge semiconductor detector to obtain fluorescence XANES spectra. Sb_2O_3 (Fluka) diluted by boron nitride and $Sb(OH)_6^-$ solution were used as reference materials for Sb XANES analysis. All measurements of solid samples were conducted at 70 K using a cryostat with closed cycle refrigerator system to prevent unexpected oxidation due to the X-ray radiation effect. The energy calibration was made using the white line peak maximum of Sb_2O_3 at 4.697 keV for Sb.

3. Results and discussion

3. 1. XRD analysis of solid samples

The XRD results from the collected samples are shown in Fig. 1. Some peaks gradually appeared from T_R = 1.0 h, and the characteristic (001), (002), and (003) lines of sulphate green rust ($GRSO_4$) can be clearly seen in the samples after 1.5 h of oxidation. These lines correspond to the crystallographic plane spacing of 11.2 Å, 5.58 Å, and 3.77 Å of $GRSO_4$ (Vins et al., 1987). All the other peaks in T_R = 1.5 h (sample name: $GR^{1.5}$) can also be assigned to $GRSO_4$, and there is no evidence for the presence of magnetite (Fe_3O_4). The (001), (002), and (003) peaks become slightly more intense and sharper over 2.0 h of oxidation, and a similar pattern is observed for other less intense green rust peaks such as the (100), (101), and (103). These findings suggest that, to a greater extent, green rust becomes crystalline as it ages. Although a lepidocrocite peak (120) starts to grow up in $GR^{2.5}$ (most aged sample; T_R = 2.5 h), the peak is very small and broad compared with the $GRSO_4$ peaks, indicating that lepidocrocite is a minor component of Fe species in $GR^{2.5}$. Thus, these findings and XRD results suggest that Fe mainly exists as green rust in all the samples, and that its crystallinity increases with T_R, indicating that most of the added Sb is expected to be adsorbed on green rust.

3. 2. Sb L_I-edge XANES analysis

Figure 2 shows the normalized Sb L_I-edge XANES spectra for the reference materials ($Sb^{III}_2O_3$ and $Sb^{V}(OH)_6^-$ solution) and green rust samples at various T_R. It is obvious from the results of the reference materials that the absorption edge shifts to higher energy for Sb species at higher oxidation state. This suggests that the position of the XANES peak can be used to distinguish Sb(III) and Sb(V). In all the samples, the Sb(III) and Sb(V) peaks are observed on their XANES spectra. Although the peak for Sb(III) species are not distinctive in the original spectra for the samples, subtraction of contribution of Sb(V), or $Sb(OH)_6^-$, from the sample spectra produced spectra with peaks corresponding to Sb(III) species (Fig. 2). These results suggest that Sb(III) and Sb(V) co-exist in all the green rust samples, thus, indicating that the Sb(V) can be reduced to Sb(III) by $GRSO_4$. This is the first evidence that $GRSO_4$ has a potential to reduce Sb(V) to Sb(III) based on an *in situ* analysis of solid phase by XANES. The result is worthy of note considering that $GRSO_4$ does not reduce As(V) to As(III) (Randall et al., 2001) and that other Fe hydroxides such as goethite and lepidocrocite, on the contrary, oxidize Sb(III) to Sb(V) (Leuz et al., 2006; Belzile et al., 2001).

Following Nguyen et al. (2003), a simulation of XANES spectra was conducted for Sb on green rust samples based on the spectra of the reference materials ($Sb^{III}_2O_3$ and $Sb^{V}(OH)_6^-$ solution) to quantitatively estimate Sb(III) and Sb(V) compositions (Fig. 3). This fitting procedure was performed within the range of 4.690-4.715 keV. In all the samples, 23-26% of Sb adsorbed on $GRSO_4$ was present as Sb(III), and a systematic trend was not shown

between T_R and the Sb(III)/Sb(V) ratio in $GRSO_4$ (Fig. 4a). These findings suggest that the crystallinity of solid does not significantly influence the potential to reduce Sb(V).

3. 3. Water phase analysis by HPLC-ICP-MS

Figures 4b and 4c show the Sb(III)/Sb(V) ratio for dissolved Sb species determined by HPLC-ICP-MS and the concentration of dissolved Fe and Sb in solution, respectively. Abundance of dissolved Fe decreased linearly with T_R, and only ca. 20% of total Fe in the system (11200 mg/dm^3 if all dissolved) remained in the solution at T_R = 2.5 h (Fig. 4c). These facts show that the dissolved Fe was consumed by the formation of $GRSO_4$ as T_R increases, and that the oxidation rate of soluble Fe(II) (= formation rate of $GRSO_4$) was approximately at the same order throughout the reaction period. Compared with Fe concentration, initial levels of dissolved Sb were relatively low; ca. 1% of total available Sb remained in solution at 10 min after Sb addition (T_R = 1.0 h), indicating that most of added Sb (99% of total Sb) were immediately adsorbed to $GRSO_4$ after its addition in the system. Subsequently, abundance of dissolved Sb gradually decreased with time (Fig. 4c). From HPLC-ICP-MS analysis, Sb(III) was observed at any T_R, and the Sb(III) fraction in dissolved species ranged from 6.3% to 14.1% in all the samples (Fig. 4b). In the control sample (system without green rust), the dissolved Sb(III) cannot be observed within the reaction period of this study (for 2.5 h) (data not shown). These results suggest that the Sb(III) observed in the Sb/green rust system is derived from the reduction by $GRSO_4$, which is consistent with the presence of Sb(III) in the solid phase shown by XANES analysis (Section 3. 2).

Green rust ($Fe_y^{II}Fe_x^{III}(OH)_{3x+2y-2z}(SO_4)_z$) is a mixed Fe(II)-Fe(III) oxyhydroxide mineral that is thought to occur under the reducing and mildly alkaline conditions found in reductomorphic soils and certain sedimentary horizons (Génin et al., 1998; Kumar et al., 1999). Consequently, it is likely to be one of the most important Fe(II) bearing minerals in immature sediments and soils. Green rust has been previously shown to reduce Se(VI) to Se(0) and nitrate to ammonium. In addition, it is also reported that green rust does not reduce As(V) to As(III). Thus, the reducing potential of green rust depends on the reactant species. In this study, we discussed for first time the interaction between Sb(V) and $GRSO_4$ based on both solid and liquid phases analyses using XAFS and HPLC-ICP-MS. It was shown that green rust has high affinity with Sb(V), and that Sb(V) was reduced to more toxic Sb(III) by green rust despite the high stability of the Sb(V) species. Thus, it is suggested that green rust may play an important role in the behavior of Sb in suboxic environment where green rust is formed. It is reported that the Sb(V) is stable form as Sb species even under reducing condition in the environment, and that the reduction of Sb(V) in the environment discussed above depends on the kinetic effect in its reaction (Cutter, 1992;

Mitsunobu et al., 2006). Therefore, green rust can be one of the important reducing agent for Sb, which can greatly influence Sb mobility in suboxic environments.

References

Belzile, N., Chen, Y.- W., Wang, Z., 2001. Oxidation of antimony (III) by amorphous iron and manganese oxyhydroxides. Chem. Geol. 174, 379-387.

Bigham, J. M., Tuovinen, O. H., 1985. In: Planetary Ecology; Caldwell, D. E., Brierley, C. L. (Eds.). Van Nostrand Reinhold Co., New York, pp. 239-250.

Chen, Y.- W., Deng, T. L., Filella, M., Belzile, N., 2003. Distribution and early diagenesis of antimony species in sediments and pore water of freshwater lakes. Environ. Sci. Technol. 37, 1163-1168.

Council of the European Communities. 1976. Council Directive 76/ Substances Discharged into Aquatic Environment of the Community. Official Journal L 129, pp 23-29.

Cutter, G. A., 1992. Kinetic controls on metalloid speciation in seawater. Mar. Chem. 40, 65-80.

Filella, M., Belzile, N., Chen, Y.- W., 2002. Antimony in the environment: a review focused on the natural waters I. Occurrence. Earth Sci. Rev. 57, 125-176.

Génin, J. –M. R., Refait, P., Olowe, A. A., Abdelmoula, M., Fall, I., Drissi, S. H., 1998. Identification of Green Rust compounds in the aqueous corrosion processes of steels; the case of Microbially induced corrosion and use of 78 K CEMS. Hyp. Int. 112, 47-50.

Hansen, H. C. B., Poulsen, I. F., 1999. Interaction of synthetic sulphate " green rust" with phosphate and the crystallization of vivianite. Clays Clay Miner. 47, 312-318

Hansen, H. C. B., Koch, C. B., Nancke-Krogh, H., Borggaard, O. K., Sørensen, J., 1996 Abiotic nitrate reduction to ammonium: key role of green rust. Environ. Sci. Technol. 30, 2053-2056.

Heasman, D. M., Sherman, D. M., Ragnarsdottir, K. V., 2003. The reduction of aqueous Au^{3+}

by sulfide minerals and green rust phases. Am. Min. 88, 725-739.

Krachler, M., Emons, H., 2001. Urinary antimony speciation by HPLC-ICP-MS. J. Anal. At. Spectrom. 16, 20-25.

Kumar, A. V. R., Singh, R., Nigam, R. K., 1999. Mossbauer spectroscopy of corrosion products of mild steel due to microbiologically influenced corrosion. J. Radioanal. Nuclear Chem. 242, 131-137.

Leuz, A.- K., Mönch, H., Johnson, C. A., 2006. Sorption of Sb(III) and Sb(V) to goethite: influence on Sb(III) oxidation and mobilization. Environ. Sci. Technol. 40, 7277-7282.

Loyaux-Lawniczak, S., Refait, P., Ehrhardt, J. J., Lecomte, P., Genic, J. –M. R., 2000. Trapping of Cr by formation of ferrihydrite during the reduction of chromate ions by Fe(II)-Fe(III) hydroxysalt green rusts. Environ. Sci. Technol. 34, 438-443.

Mitsunobu, S., Harada, T., Takahashi, Y., 2006. Comparison of antimony behavior with arsenic under various soil redox conditions. Environ. Sci. Technol. 40, 7270-7276.

Myneni, S. C. B., Tokunaga, T. K., Brown, Jr. G. E., 1997. Abiotic selenium redox transformations in the presence of Fe(II, III) oxides. Science 278, 1106-1109.

Nguyen, D. L., Taarit, Y. B., Millet, J. –M. M., 2003. Determination of the oxidation state of antimony, iron and vanadium in mixed vanadium and iron antimonite oxide catalysts. Catal. Lett. 90, 65-70.

Nomura, M., Koyama, A., 2001. Performance of a beamline with a pair of bent conical mirrors. Nucl. Instrum. Methods Phy. Res. Sect. A 467, 733-736.

O'Loughlin, E., Kelly, S. D., Cook, R. E., Csencsits, R., Kemner, K. M., 2003. Reduction of uranium(VI) by mixed iron(II)/iron(III) hydroxide (green rust): formation of UO_2 nanoparticles. Environ. Sci. Technol. 37, 721-727.

Picard, C., Bosco, M., 2003. Soil antimony pollution and plant growth stage affect the biodiversity of auxin-producing bacteria isolated from the rhizosphere of Achillea ageratum L. FEMS Microbiol. Ecol. 46, 73-80.

Randall, S. R., Sherman, D. M., Ragnarsdottir, K. V., 2001. Sorption of As(V) on green rust

($Fe_4(II)Fe_2(III)(OH)_{12}SO_4 \cdot 3H_2O$) and lepidocrocite (γ-FeOOH): surface complexes from EXAFS spectroscopy. Geochim. Cosmochim. Acta 65, 1015-1023.

Refait, P., Abdelmoula, M., Génin, J. –M. R., 1998. Mechanisms of formation and structure of green rust one in aqueous corrosion of iron in the presence of chloride ions. Corros. Sci. 40, 1547-1560.

Scheinost, A. C., Rossberg, A., Vantelon, D., Xifra, I. O., Kretzschmar, R., Leuz, A. –K., Funke, H., Johnson, C. A., 2006. Quantitative antimony speciation in shooting-range soils by EXAFS spectroscopy. Geochim. Cosmochim. Acta 70, 3299-3312.

Schwertmann, U., Fechter, H., 1994. The formation of green rust and its transformation to lepidocrocite. Clay Miner. 29, 87-92.

Su, C-M, Puls, R. W., 2004. Significance of iron(II,III) hydroxycarbonate green rust in arsenic remediation using zerovalent iron in laboratory column tests. Environ. Sci. Technol. 38, 5224-5231.

United States Environmental Protection Agency. 1979. Water Related Fate of the 129 Priority Pollutants. Doc. 745-R-00-007, USEPA, Washington, DC, Vol. 1.

Vins, J., Subrt, J., Zapletal, V., Hasousek, F., 1987. Preparation and properties of green rust type substances. Coll. Czech. Chem. Comm. 52, 93-102.

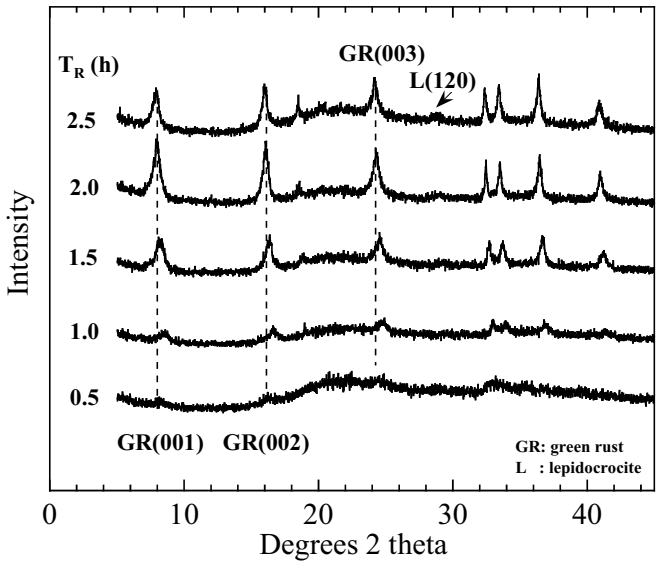

Fig. 1. XRD analysis of solid materials collected from the suspension.

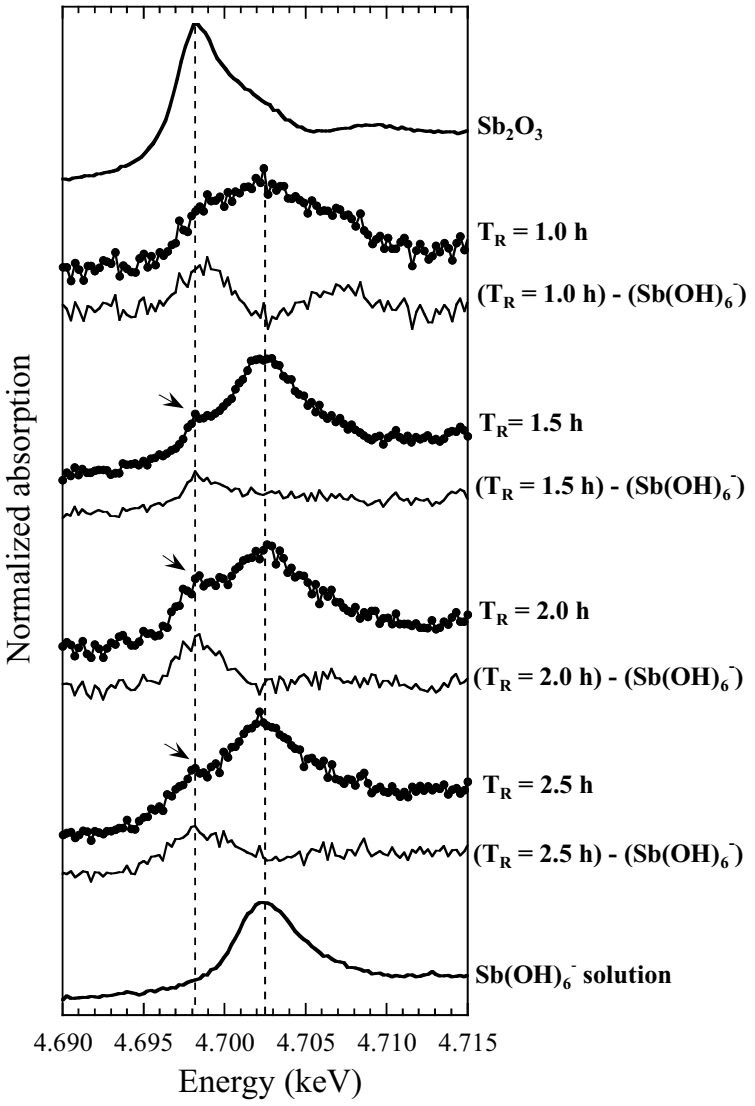

Fig. 2. Normalized Sb L_I-edge XANES spectra of the reference materials (Sb_2O_3 and $Sb(OH)_6^-$solution) and Sb adsorbed on green rust. All the spectra of the samples were measured at 70 K to prevent unexpected oxidation during XANES analysis. Arrows in figure show the peak related to Sb(III) in the XANES spectra of the samples.

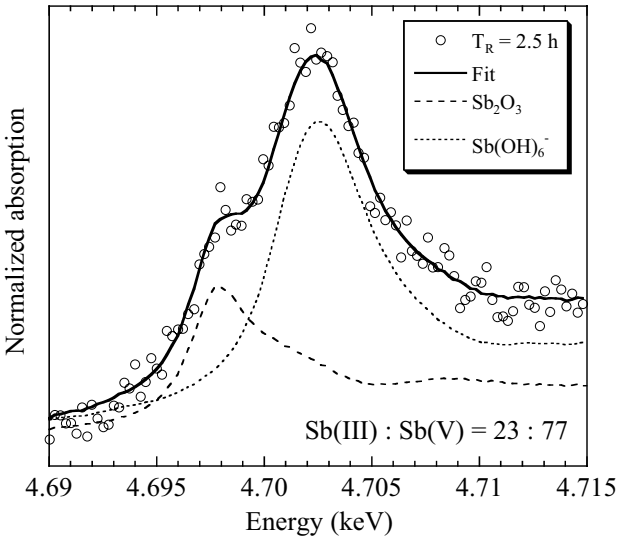

Fig. 3. Linear combination fitting result for Sb L_I-edge XANES spectrum of the green rust sample (T_R = 2.5 h) with Sb_2O_3 and $Sb(OH)_6^-$ solution.

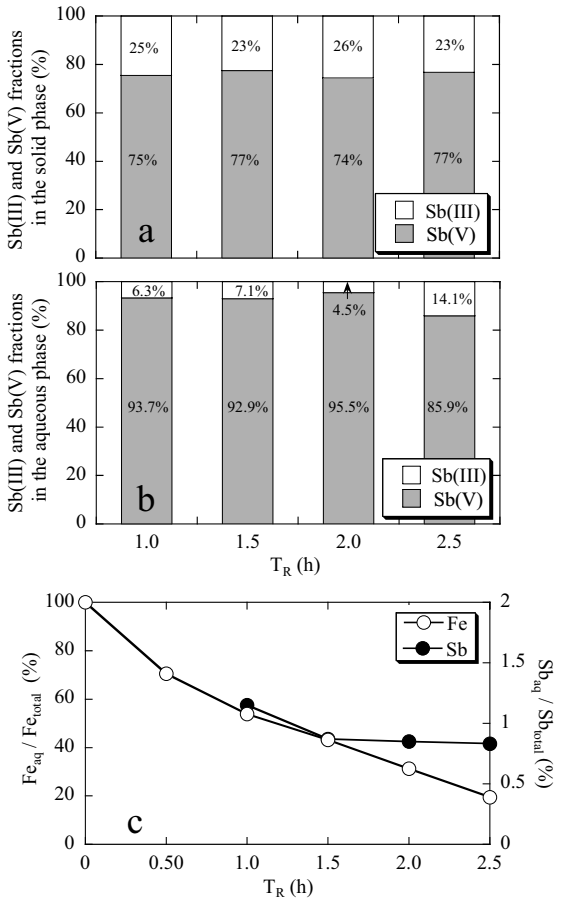

Fig. 4. (a) Sb(III)/Sb(V) ratio in green rust samples by the simulation of Sb L_I-edge XANES at various T_R. (b) Sb(III)/Sb(V) ratio for dissolved Sb species at various T_R by HPLC-ICP-MS analysis. (c) Dissolved concentrations of Fe and Sb at various T_R. In (a) and (b), the numerical values in each bar stand for the percentages of Sb(III) and Sb(V). Uncertainties of Fe and Sb in (c) are smaller than the sizes of the symbols.